FEOTS v0.0.0: A New Offline Code for the Fast Equilibration of Tracers in the Ocean

Joseph Schoonover[1], Wilbert Weijer[2], and Jiaxu Zhang[3,4]

[1]Fluid Numerics LLC., Boulder, CO 80304
[2]Los Alamos National Laboratory, Los Alamos, NM 87545
[3]Cooperative Institute for Climate, Ocean, and Ecosystem Studies, University of Washington, Seattle, WA 98105
[4]NOAA/Pacific Marine Environmental Laboratory, Seattle, WA 98115

Correspondence: Joseph Schoonover (joe@fluidnumerics.com)

Abstract. In this paper we introduce a new software framework for the offline calculation of tracer transport in the ocean. The Fast Equilibration of Ocean Tracers Software (FEOTS) is an end-to-end set of tools to efficiently calculate tracer distributions on a global or regional sub-domain using transport operators diagnosed from a comprehensive ocean model. To the best of our knowledge, this is the first application of a Transport Matrix Model to an eddying ocean state. We demonstrate the capabilities of FEOTS in an application focused on the Argentine Basin, where intense eddy activity and the Zapiola Anticyclone lead to strong mixing of water masses. The demonstration clearly shows the benefits of the approach, while at the same time highlighting the limitations of the Impulse Response Functions approach in capturing tracer transports by a non-linear advection scheme. Our future work will focus on improving the computational efficiency of the code to reduce time-to-solution, and on using different basis functions to better represent non-linear advection operators.

1 Introduction

Many oceanographic research problems involve the transport and distribution of tracers that do not feed back on the ocean dynamics. Examples of such problems are the diagnostic tracking of water masses using passive tracers (e.g., Dukhovskoy et al., 2016; Zhang et al., 2021); validating the use of isotopes or grain size distributions in marine sedimentary records to infer past ocean circulation changes (e.g., Jahn et al., 2015; Zhang et al., 2017; Gu et al., 2019; Missiaen et al., 2020); assessing anthropogenic carbon uptake by the ocean (e.g., Sarmiento et al., 1992; Khatiwala et al., 2009; Wang et al., 2012); studying the evolution of marine biogeochemical systems (e.g., Séférian et al., 2020); or tracking the fate of microplastics in the ocean (e.g., Mountford and Morales Maqueda, 2019). In many cases, the transport of these tracers is dominated by mesoscale processes like eddies. Typical ocean climate models use grids that are too coarse to explicitly resolve these processes and rely on parameterizations to simulate their impact on tracer fields; but it has become clear that these eddy-parameterized models fail to reproduce some critical aspects of the real ocean (e.g., Lozier, 2010). What is more, the ocean also contains *dynamical* features that rely on mesoscale eddies, and which cannot be reproduced by low-resolution models.

A case in point is the Argentine Basin. It is among the most turbulent regions in the World Ocean (Fu and Smith, 1996), mostly on account of the confluence of two western boundary currents, the Brazil and Malvinas Currents (e.g., Garzoli, 1993).

A seamount in the center of the basin is associated with a local minimum in eddy kinetic energy (Fu and Smith, 1996), but is surrounded by a very strong barotropic vortex, the Zapiola Anticyclone (ZA; Saunders and King, 1995; de Miranda et al., 1999). This anticyclone is understood to be driven by the intense eddy field (Dewar, 1998), and has been shown to inhibit exchanges between the interior of the ZA and its surroundings (Weijer et al., 2015, 2020). Strikingly, the Argentine Basin is also a main conduit of water mass exchange between the Atlantic and Southern Oceans (e.g., Jullion et al., 2010), so eddy-driven mixing of water masses in the Argentine Basin may have implications for the global thermohaline circulation. It is clear that studying tracer transport and mixing in the Argentine Basin requires an ocean model that resolves the ocean's mesoscale; not just to accurately represent the transports by narrow boundary currents and the turbulent eddy field, but also to generate the ZA in the first place. Second, the equilibration of tracers at deeper levels may take many decades or centuries, requiring a model capability that can be run for such long times, or can determine equilibria directly using iterative solvers. Third, this problem is ideally addressed using a representation of the global ocean circulation; not only so that the ocean circulation in the region of interest is fully consistent with large-scale oceanographic drivers, but also for the practical reason that not every regional problem would require a unique model configuration.

The cost and technical challenges of running global and fully-dynamic ocean models make it expensive and difficult at best, but often impossible, to address problems like these. It is obvious that there is a need for simple and efficient tools that solve tracer transport and distribution problems, without the need to explicitly simulate ocean dynamics. In the past decade or so, several Transport Matrix Models (TMMs) have been developed that allow for the simulation of passive tracers in a stand-alone (offline) code, using transport operators that have been diagnosed from comprehensive ocean models (Primeau, 2005; Khatiwala et al., 2005; Khatiwala, 2007; Bardin et al., 2014). In particular, Khatiwala et al. (2005) pioneered the approach of empirically estimating an ocean model's transport processes by diagnosing the action of the transport (advection and diffusion) operators on simple basis functions like impulse fields. The resulting Impulse Response Functions (IRFs) can straightforwardly be converted to the desired transport matrices. This process requires minimal intervention in the parent model.

Climate models have generally been trending towards higher resolution as computational resources continue to expand. Simulations are now routinely being produced at eddy permitting and eddy resolving scales. To the best of our knowledge, the capability introduced in this paper is the first TMM developed for and applied to eddying ocean states, with transport operators diagnosed from a global ocean model with nominal resolution of $0.3°$ and 100 vertical levels ($\sim 10^8$ degrees of freedom).

Our computational framework is embodied in the Fast Equilibration of Ocean Tracers Software (FEOTS; https://github.com/LANL/FEOTS). FEOTS generalizes the methodology from Bardin et al. (2014) by providing an end-to-end set of tools that i) use an advanced optimization algorithm to generate an optimal set of impulse functions, given the grid layout and operator stencils for the parent model; ii) transform the resulting IRFs obtained from the parent model to transport operators; iii) set up regional or global tracer problems, with different types of tracers; iv) run forward simulations of the offline tracer model; and v) use a Newton-Krylov solver to determine steady tracer distributions. The framework is applied here to the Parallel Ocean Program (POP; Smith et al., 2010); but the design is flexible enough to be generally applicable –in particular to the new generation of ocean models with unstructured grids, like the Ocean Model for Prediction Across Scales (MPAS-Ocean, Ringler et al., 2013).

In this paper we present validation and verification results for the FEOTS offline tracer solver in a regional forward simulation configuration focused on the Argentine Basin. Specifically, we will show that uniform tracer fields are preserved within 0.01% after five years of offline model integration and implemented time integration schemes exhibit the expected convergence rates. Additionally, we will present a comparison of the offline regional tracer simulation using five-day averaged transport operators with an online tracer simulation from the parent model.

2 Methodology

Our work builds on the methodologies of Bardin et al. (2014) to create FEOTS. This application is used to aid in the capturing of transport operators from ocean model simulations and in the execution of offline regional transient tracer simulations. In section 2.1 we present the governing equations for a non-interacting passive-tracer system and outline the methodology for capturing transport operators from a comprehensive ocean model in 2.2. The offline forward stepping algorithm and treatment of vertical mixing is presented in section 2.3. In section 2.4 we discuss the parent model POP, while the Argentine Basin test problem is defined in 2.5.

2.1 Governing Equations

We model a passive dye tracer as a concentration field that is subjected to advection and diffusion,

$$\frac{\partial c}{\partial t} + \nabla \cdot (\boldsymbol{u}c - \mathbb{K}\nabla c) = 0 \tag{1}$$

where c is the tracer concentration, t is time, $\boldsymbol{u}$ is the ocean velocity field, and $\mathbb{K}$ is the diffusivity tensor that models unresolved eddy activity. The initial and boundary conditions are set to be

$$c(t=0) = c_0(z, \theta, \phi) \tag{2}$$

and

$$c = c_b(z, \theta, \phi, t), \tag{3}$$

where z is depth (measured positive downward), θ is longitude, and ϕ is latitude. The semi-discrete form of (1) can be written as:

$$\boldsymbol{c}_t + (A + D_h + D_v)\,\boldsymbol{c} = 0 \tag{4}$$

where $\boldsymbol{c}$ is a vector of the discrete values of the tracer, A is the advection matrix, D_h is the horizontal diffusion matrix, and D_v is the vertical diffusion matrix.

The transport operators in equation (4) can be diagnosed empirically from a comprehensive ocean model, the "parent model", using the methodology used by Bardin et al. (2014) and pioneered by Khatiwala et al. (2005). In the parent model, passive tracers are initialized to a set of impulse functions $[\boldsymbol{c}^{(i)}]_{i=1}^{M}$ at the beginning of each time step, where M is the number of

impulse functions. At the end of each time step, the tendency of the impulse function, called the impulse response function (IRF) is captured by diagnosing the advective tendency,

$$\boldsymbol{R}^{(i,n)} = A^{(n)}\boldsymbol{c}^{(i)} \tag{5}$$

90   where $\boldsymbol{R}^{(i,n)}$ is the impulse response function at time level n associated with impulse function i, $A^{(n)}$ is the transport matrix at time level n, and $\boldsymbol{c}^{(i)}$ is the ith impulse function. The IRFs are averaged over a certain averaging period and written out to file.

2.2   Graph Coloring approach to Operator Diagnosis

The purpose of capturing the impulse response functions is to diagnose sparse matrices that are consistent with the advection
95   discretization in the parent model. To illustrate this procedure, suppose that the parent model has N grid cells and that N impulse fields are set as the Kronecker delta functions:

$$[\boldsymbol{c}^{(i)}]_{i=1}^{N} = [\delta_{j,i}]_{i=1}^{N} \tag{6}$$

In this setup, impulse function i is zero at all grid cells except for grid cell i where the impulse function has a value of one. Application of the transport matrix to each of the $\boldsymbol{c}^{(i)}$ returns column i of A,

$$100 \quad A\boldsymbol{c}^{(i)} = \sum_{j=1}^{N} A_{m,j}\delta_{j,i} = A_{m,i} \quad \text{for } m = 1,2,3,...,N \tag{7}$$

While using a set of Kronecker delta functions will completely diagnose all of the elements of the transport matrix, this strategy is computationally expensive. For each time step, this strategy requires computing the advective tendency for N tracer fields, where N is the number of grid cells. For example, coarse resolution model at $\mathbb{O}(1°)$ resolution have roughly 10^6 grid cells. Storing 10^6 impulse and impulse response functions would require approximately 3 TB of memory at double precision.

105   To reduce the number of required impulse functions to fully diagnose the transport matrices, we can take advantage of the fact that the advection scheme results in a sparse matrix. Equivalently, the domain of influence of the advection operator is limited to nearby grid cells. The parent model employed in Bardin et al. (2014) used a third order upwind scheme, where the impulse response is guaranteed to extend no further than two grid-cells in each spatial dimension. Because of this, the authors used a set of 125 tracer fields,

$$110 \quad c(i,j,k;i_0,j_0,k_0) = \delta_{i0,i(mod5)}\delta_{j0,j(mod5)}\delta_{k0,k(mod5)} \quad \text{for } i_0 = 1,...,5; j_0 = 1,...,5; k_0 = 1,...,5 \tag{8}$$

FEOTS offers a unique capability to generate a minimal set of impulse functions by posing the problem as a graph coloring problem. A graph $G(V,E)$ is defined by a set of vertices V and edges E that connect the vertices. Two vertices connected by an edge are said to be adjacent. A valid graph coloring of $G(V,E)$ assigns colors to each vertex so that no two adjacent vertices have the same color. To calculate impulse functions that can be used to diagnose transport operators, FEOTS offers
115   functionality to express a POP mesh and an advection stencil into an equivalent graph that is colored with a Greedy algorithm.

4

Method	c^*
Forward Euler	c^n
Adams-Bashforth 2nd Order	$\frac{3c^n - c^{n-1}}{2}$
Adams-Bashforth 3rd Order	$\frac{23c^n - 16c^{n-1} + 5c^{n-2}}{12}$

Table 1. Optional values for c^* in Eq. (10), based on the choice in time integration scheme.

This formulation has the benefit that it can be generalized to parent models based on unstructured grids and it takes into account irregular boundaries from variable bathymetry.

In FEOTS, graph vertices V correspond to each ocean grid cell, centered on tracer points, in the POP mesh. Two vertices are adjacent if their impulse response functions overlap. Because a valid coloring results in adjacent vertices having distinct colors, vertices with the same color can safely be assigned to the same impulse function. Consequently, the chromatic number of the graph corresponds to the number of impulse functions used for model diagnosis. For this work, the parent model uses a $0.3°$ periodic tripole mesh and the 3rd order flux-limited Lax-Wendroff advection scheme. This approach results in 53 impulse functions required to uniquely diagnose the transport operators.

2.3 Time integration

Forward integration of the offline tracer model uses Backward Euler for vertical mixing and can use Forward Euler, Adams-Bashforth 2nd Order, or Adams-Bashforth 3rd Order for transport. As in Bardin et al. (2014), we forward step an equation for the volume anomaly using a forward Euler method. Volume anomalies arise due to divergence in the transport field at the upper-most z-level that are associated with fluctuations of the free-surface.

In general, the time integration scheme can be written as

$$\boldsymbol{v}^{n+1} = \boldsymbol{v}^n + \Delta t \mathbb{A}^n \boldsymbol{i} \tag{9}$$

$$(\mathbb{I} + \mathbb{V}^{n+1} + \mathbb{D}_v)\boldsymbol{c}^{n+1} = (\mathbb{I} + \mathbb{V}^n)\boldsymbol{c}^n + \Delta t(\mathbb{A} + \mathbb{D}_h)\boldsymbol{c}^* \tag{10}$$

where $\boldsymbol{c}^*$ depends on the time integration scheme that is used (Table 1) and $\mathbb{V}^{n+1}$ is a diagonal matrix whose diagonal elements are the volume anomalies.

In ocean models, advection and horizontal diffusion operators have a compact stencil, enabling the use of the IRF approach described in the previous section to 'capture' these advection and diffusion operators. However, vertical diffusion is usually treated differently, by solving a tri-diagonal system that touches the entire water column. The reason is that high values of vertical diffusivity are applied where the water column is unstable; and these values easily render any explicit scheme unstable. Consequently, as the region of influence of the vertical diffusion operator is the entire water column, the IRF approach would demand a separate IRF field for each vertical level of the model grid, which is prohibitive for finely resolved grids. Instead, FEOTS treats the vertical solve similarly as the parent model, so rather than IRFs, the vertical diffusivities are diagnosed, saved, and used to recreated the vertical diffusion operators offline.

5

Forward stepping FEOTS requires inverting a tri-diagonal system of equations, given by equation (10), for the tracer concentration in order to incorporate vertical mixing. To solve this system, we use the preconditioned conjugate gradient algorithm (Shewchuk, 1994) with a diagonal preconditioner. The initial solution guess for the vertical mixing solver is set as the tracer concentration that is predicted without vertical mixing,

$$\boldsymbol{c}_0^{n+1} = (\mathbb{I} + \mathbb{V}^{n+1})^{-1}((\mathbb{I} + \mathbb{V}^n)\boldsymbol{c}^n + \Delta t(\mathbb{A} + \mathbb{D}_h)\boldsymbol{c}^*) \tag{11}$$

The conjugate gradient solver is stopped when the residual magnitude, relative to the initial solution guess magnitude, is less than 10^{-6}.

2.4 Parent Model

FEOTS is used for offline tracer simulations using transport operators diagnosed from a comprehensive ocean model, the "parent model". Here we apply FEOTS to the Parallel Ocean Program, in the framework of the E3SMv0-HiLAT climate model (Hecht et al., 2019). Our specific configuration is described in Zhang et al. (2019). It has a tripole grid with nominal 0.3° spatial resolution. The grid has 1200x800 grid cells, and 100 levels in the vertical. The grid has a 'seam' in the Arctic that connects the poles in Siberia and in Canada. Although technically not eddy-resolving in most of the World Ocean (Hallberg, 2013), this configuration has a vigorous eddy field, and a realistic representation of the eddy-driven Zapiola Anticyclone in the Argentine Basin (Weijer et al., 2020).

With $\mathbf{O}(10^8)$ degrees of freedom, and an eddying field that requires transport operators at high temporal frequency (e.g., 5-daily averages), the data volume of the diagnosed IRFs can become unmanageable quickly. It is therefore critical to keep the number of IRFs to an absolute minimum. This means that we need to choose advection and diffusion treatments that have the most compact stencils. Typically high-resolution ocean models use a bi-harmonic mixing scheme to dampen out the dispersive errors caused by the advection operator (e.g., Hecht et al., 2008). Bi-harmonic mixing is clearly undesirable for our application, given its huge stencil. Of the three advection schemes currently implemented in POP (Smith et al., 2010), the centered and 3rd-order upwind schemes require explicit diffusion to manage the dispersion error. The flux-limited Lax-Wendroff scheme does not, making this the only reasonable choice for our application; even though its stencil is quite large (27 grid points, $3 \times 3 \times 3$) compared with the other two (7 grid points for centered, 13 for the 3rd-order upwind scheme). This choice requires 53 impulse functions to capture the advection operator (compared to 34 impulse functions for the 3rd-order upwind scheme), but eliminates the need for explicit diffusion. The downside of this choice is that the non-linearity of the advection scheme violates the basic assumption that the advection operator preserves tracer correlations, or more specifically the assumption:

$$A^{(n)}\left(\boldsymbol{c}^{(i)} + \boldsymbol{c}^{(j)}\right) = A^{(n)}\boldsymbol{c}^{(i)} + A^{(n)}\boldsymbol{c}^{(j)} \tag{12}$$

when $\boldsymbol{c}^{(i)}$ and $\boldsymbol{c}^{(j)}$ have non-zero values in adjacent grid cells. In other words, the flux limiting has a stronger impact on the spiky impulse fields than on the smooth tracer fields that they are collectively meant to represent. This will lead to stronger diffusion, which will be apparent and quantified when comparing the online and offline simulations in subsection 3.2.

The model is forced by the normal-year CORE-II climatology (Coordinated Ocean-Ice Reference Experiments version 2; Griffies et al., 2012), which has been a widely used framework to force ocean and/or sea ice models for hindcast simulations. We

175 ran the model for 5 years, after a 63-year spin-up, and diagnosed 5-day averaged IRFs and vertical diffusivities. We repeated the simulation for 105 days, diagnosing 1-day averaged IRFs. The data volume of the five years' worth of 5-day averaged operators (IRFs and diffusivities) is about 9 TB. Once transformed to transport operators, the data volume is 4 TB.

2.5 The Argentine Basin Test Problem

As discussed in the introduction, the Argentine Basin is an ideal region for testing a tracer transport capability in an eddying
180 ocean model. In this paper we compare online and offline simulations of dye tracers that are initialized at the boundaries of the Argentine Basin, here chosen as $[52.18^o S, 28.06^o S] \times [70.25^o W, 24.90^o W]$. In all simulations, the only source of tracers comes from the model boundary conditions applied along the southern, eastern, and northern boundaries.

We want to distinguish between water masses that originate from each of the domain boundaries and above and below 1000 m depth. This is accomplished by simulating six passive tracer fields D_i with boundary conditions:

185 $$D_1 : c_b^1 = H(1000 - z) \text{ when } \phi = 52.18^o S \tag{13a}$$

$$D_2 : c_b^2 = H(z - 1000) \text{ when } \phi = 52.18^o S \tag{13b}$$

$$D_3 : c_b^3 = H(1000 - z) \text{ when } \theta = 24.90^o W \tag{13c}$$

$$D_4 : c_b^4 = H(z - 1000) \text{ when } \theta = 24.90^o W \tag{13d}$$

$$D_5 : c_b^5 = H(1000 - z) \text{ when } \phi = 28.06^o S \tag{13e}$$

190 $$D_6 : c_b^6 = H(z - 1000) \text{ when } \phi = 28.06^o S \tag{13f}$$

where $H(x)$ is the Heaviside step function. With this configuration, tracers D_1, D_3, and D_5 are released in the upper 1000 m, on the southern, eastern, and northern boundaries, respectively; while tracers D_2, D_4, and D_6 are released below 1000 m.

3 Results

In this section, we present results of an offline regional study focused on the Argentine Basin. We first present verification of
195 the constant preservation property (subsection 3.1). Then we present a comparison of the tracer simulation results in the parent model (online) and the offline model using 5-day averaged transport operators (subsection 3.2), followed by a comparison between 1-day and 5-day averaged transport operators (subsection 3.3). Finally, we will discuss the computational performance of the code (subsection 3.4) on the systems where our simulations were conducted.

3.1 Constant Preservation

200 The parent model uses a finite volume discretization that guarantees the preservation of constant tracer fields. To verify that FEOTS accurately diagnoses transport operators that are representative of the parent model, our first simulation involves verifying that a constant tracer field remains constant under the action of the diagnosed transport operators.

7
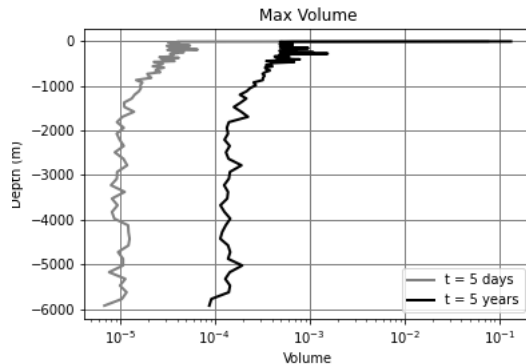
Figure 1. Vertical profile of the max volume anomaly after 5 days (gray) and after 5 years (black). In the exact form of the equations, the volume anomaly should only exist in the first vertical layer at the ocean surface. Non-zero values in the volume beneath the surface layer arise due to round-off errors.

In all of our simulations, we have opted to use single precision arithmetic and have enabled aggressive compiler optimizations (compiler option *-Ofast* with GCC 9.2.0). These choices were made to minimize data storage costs for the transport operators and post-processing output and to optimize the time-to-solution for the offline simulations. Although analytically, we expect that the FEOTS algorithm should preserve constant tracer fields, errors from floating point arithmetic are expected to be the main source of constant preservation errors.

To better understand the spatial distribution and the relative impact of round-off errors, we configure a simulation where the initial tracer field is set to $s_0 = 1$ and there is no external source or sink of tracer. Since $\nabla s_0 = 0$ and $\nabla \cdot \boldsymbol{u} = 0$ under the discretizations used in the parent model, we expect that $s_t = 0$ and $s = s_0 = 1$ for all time. For this experiment, we use the 5-day average operators and forward step the model for 5 years to cycle through the 365 diagnosed transport operators once.

Figure 1 shows the maximum volume anomaly in the domain as a function of depth after five days and five years of integration. Analytically, the volume anomaly is expected to be zero in all cells except the top-most layer. At the surface layer, fluctuations in the free surface height are associated with non-zero fluid divergences that contribute to changes in the fluid volume. Beneath the surface layer, the fluid velocity field is expected to be divergence free. In general, larger errors in the volume anomaly are observed above 1000 m depth. After five days, errors in the deep ocean are $\mathbf{O}(10^{-5})$ and after five years, the deep ocean volume anomaly errors have grown by an order of magnitude to $\mathbf{O}(10^{-4})$. Larger errors are observed above 1000 m, reaching $\mathbf{O}(10^{-3})$ after 5 years. Note that the volume anomaly field is identical for all choices in time integrator for the dye tracer and is independent of vertical mixing.

Errors in the volume anomaly lead to spurious values for predicted tracer concentrations. For this simulation, any deviation of the tracer concentration from its initial uniform value is erroneous. Figure 2 shows the max error in the dye tracer as a function of depth after five days and five years of integration, with and without mixing. After five years of integration, the maximum relative error with mixing is about 0.05% and without mixing is about 0.01%. At depth, the errors in the tracer are
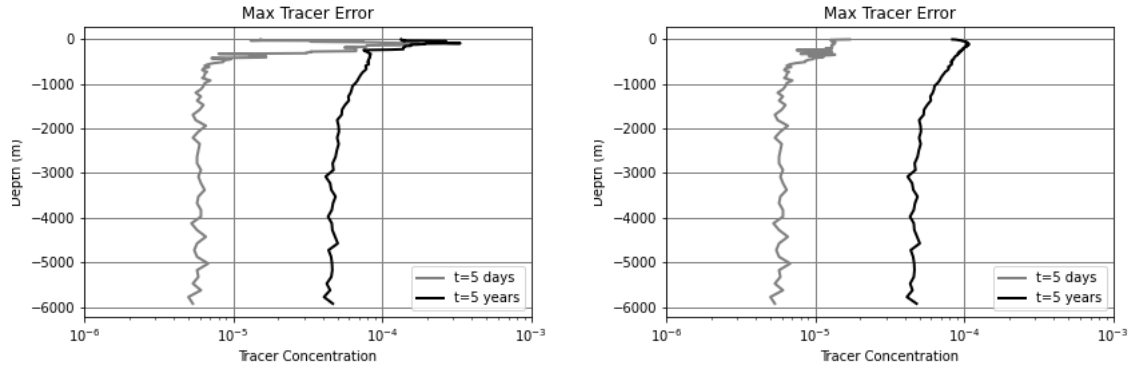
Figure 2. Vertical profile of the max error in the dye tracer after 5 days (gray) and after 5 years (black) for simulations with mixing (left) and without mixing (right). Errors that arise from integrating a uniform tracer field arise from round-off errors in volume anomaly. When mixing is enabled, vertical mixing redistributes errors and resulting in elevated errors in the upper layers in the simulation.

comparable with and without mixing. However, above 1000 m, particularly in the mixed layer, the inclusion of mixing results
225 in an accumulation of round-off errors.

3.2   The Zapiola test case: Offline vs. Online Comparison

In addition to quantifying errors for the constant-tracer scenario, a practical concern is in the comparison between the online and offline tracer simulations. The time-averaging of the transport operators will introduce differences between the online and offline simulations, as will the flux-corrected advection operator. Our aim is to quantify and qualitatively describe the
230 differences between a tracer simulation conducted directly in the online parent model and the offline model. We do this for our example problem, namely determining the source waters of the Zapiola Anticyclone.

Figure 3 compares the tracer fields obtained with the online and offline method, at the end of the 5-year analysis period. The dye tracers shown are those that are released in the upper 1000 m at each of the three domain boundaries. Visual inspection shows that the online simulation has sharper gradients compared to the offline simulation, even though the same dynamical
235 features are visible. This is a result of the non-linear advection operator that is more diffusive when applied to impulse functions than to a smooth tracer field. The advective errors also affect the inventory of dye tracers within the Zapiola Anticyclone. Figure 4 shows the vertical distribution of tracer concentrations averaged over the Zapiola Anticyclone, while Fig. 5 shows the total tracer inventories.

Dye tracer D_1, sourced at the southern boundary in the upper 1000 m, reaches the ZA after about 45 days in the online
240 simulation (Fig. 4, upper row). Inventories in the upper 1000 m rise steadily in the first 2 years; then become mostly steady, indicating saturation is reached (Fig. 5a, black dashed). Just below the surface, concentrations in the final 3 years average about 0.76, suggesting that 76% of the surface waters within the ZA may be derived from the Southern Ocean through the Malvinas Current. At 984 m this fraction is 0.45. Inventories below 1000 m increase slowly and contain 17% of the column
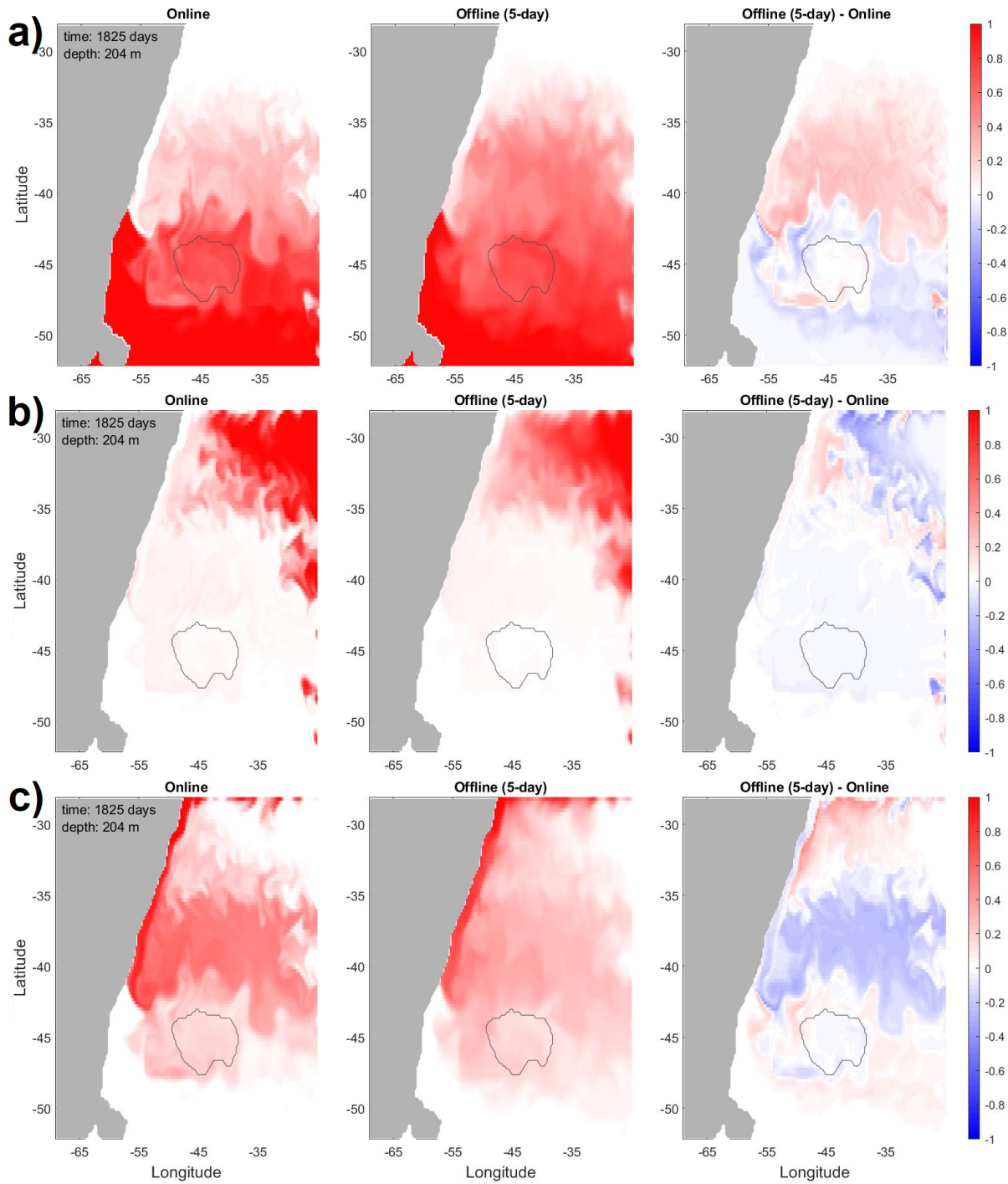
Figure 3. Online and offline tracer concentrations –and their difference– at 204 m depth, and at the end of the full 5-year period for which operators were diagnosed at 5-daily averages. Shown are dye tracers a) D_1 (sourced at the southern boundary), b) D_3 (eastern boundary), and c) D_5 (northern boundary); all sourced in the upper 1000 m. Gray contour indicates the location of the Zapiola Anticyclone.
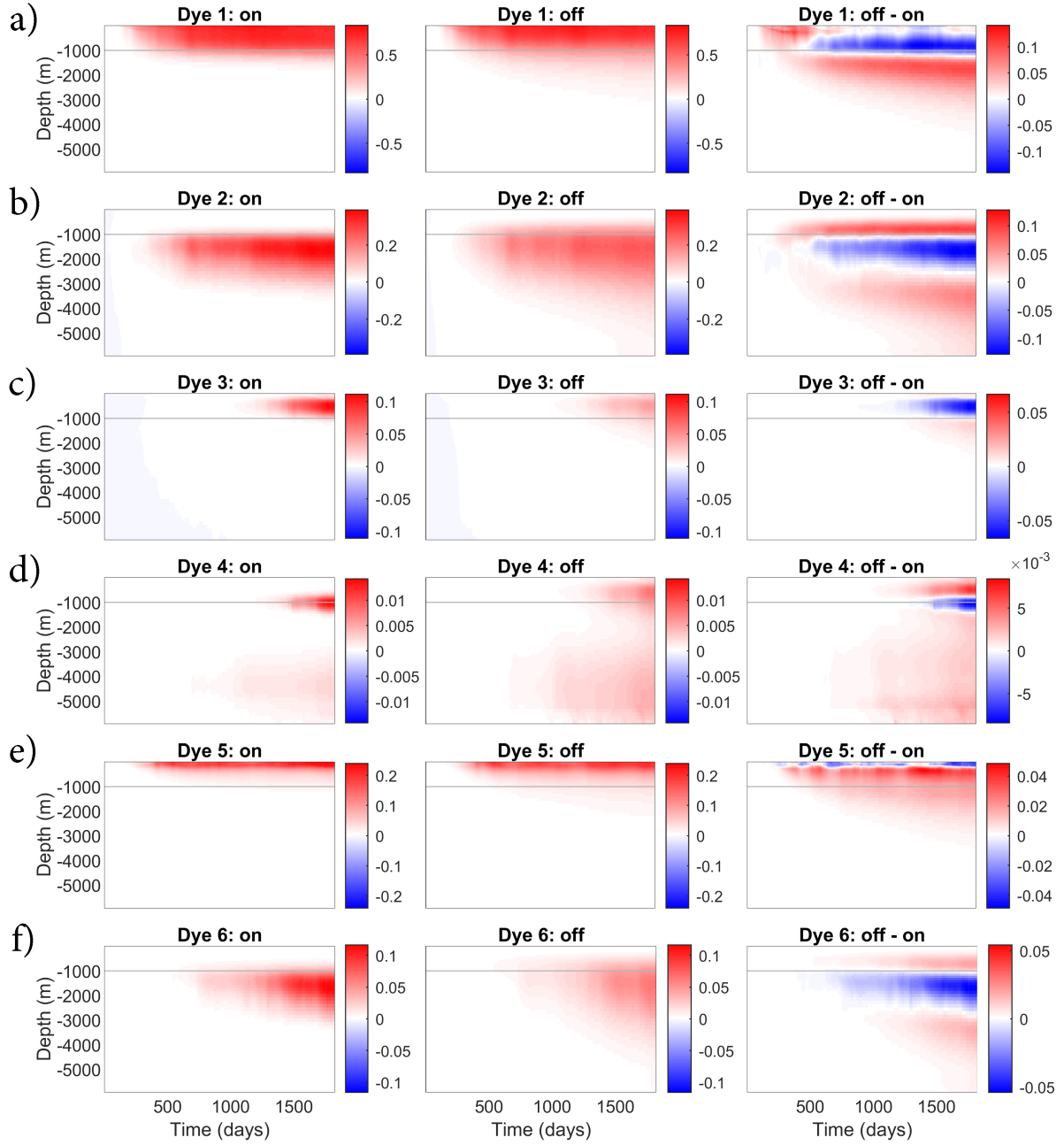
Figure 4. Hovmüller plots of the concentrations of the 6 dye tracers, averaged over the Zapiola Anticyclone; for the online (left column) and offline (center) simulations, and their difference (right). The 1000 m level is indicated by the light gray line.

11
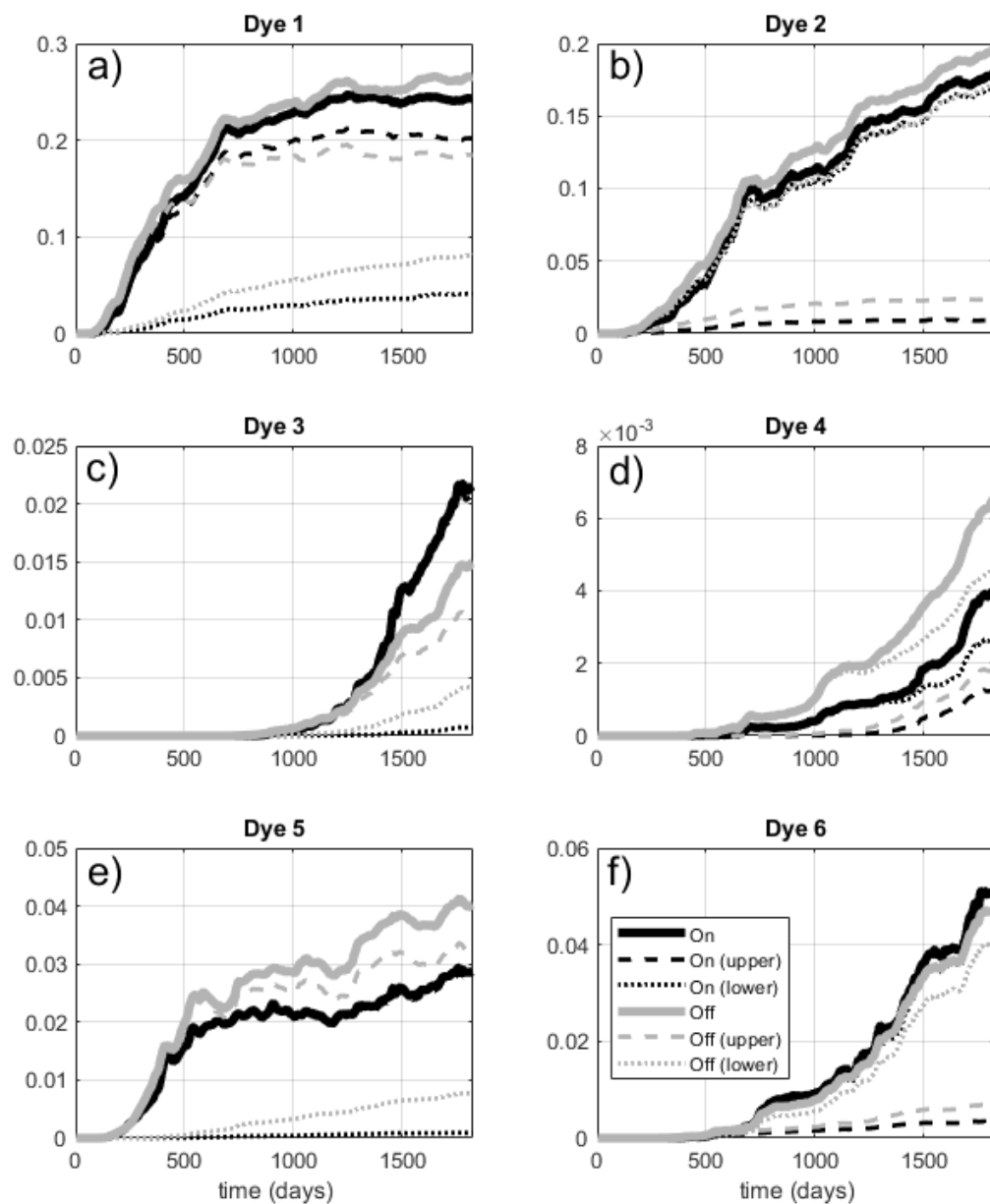
Figure 5. Total inventories (10^{15} kg) of the 6 dye tracers in the Zapiola Anticyclone, for the online (black) and offline (gray) simulations. Dashed and dotted lines are the inventories above and below 1000 m, respectively.

inventory after 5 years (Fig. 5a, black dotted). The offline simulation reproduces this behavior qualitatively, but with significant

quantitative differences. D_1 reaches the ZA about 5 days earlier and increases faster than the online simulation, but upper-layer inventories plateau at a slightly lower level (Fig. 5a, gray dashed). Tracer fraction reaches 0.74 just below the surface, close to the online simulation, but the saturation value of 0.37 at 1000 m depth is significantly lower. Figure 4 (upper row) shows that this is due to a significant vertical redistribution of tracers by vertical diffusion that depletes tracers from the upper 1000 m and increases inventories below. Indeed, the inventory below 1000 m accounts for 30% of the column inventory after 5 years.

The story is similar for dye tracer D_2, which is sourced at the southern boundary below 1000 m. It arrives in the ZA after 87 days in the online simulation. Inventories below 1000 m (Fig. 5b, black dotted) rise quickly through the first 2 years, followed by a more gradual (linear) rise after that. Tracer concentrations at 1049 m level out at 0.20 after 3 years. The total contribution of Southern Ocean waters ($D_1 + D_2$) is about 59% at 1000 m depth. The offline simulation reproduces this behavior quite well, but displays higher inventories in the upper 1000 m that increases the overall column inventory by 9% after 5 years. The vertical profiles again clearly show the impact of vertical diffusion that depletes tracers in the 1000-3000 depth range, and increases concentrations below and above (Fig. 4; second row). D_2 concentration at 1049 m depth levels out at 0.21, with a total Southern Ocean contribution at 1000 m of 56%.

The next-largest contribution to the ZA tracer inventory is coming from the north through Dye tracers D_5 (upper 1000 m) and D_6 (below 1000 m). It takes about 110 days for D_5 to arrive at the ZA, and the surface concentration saturates at about 0.18 after 550 days (as the does the upper-layer tracer inventory; Fig. 5e, black dashed, overlain by solid). This suggests that the Brazil Current may contribute about 20% of the surface waters in the ZA. At 984 m, however, this fraction is still only 0.015 after 5 years, and rising, probably reflecting the strongly sheared character of the Brazil Current, and the long transit time from the northern domain boundary to the ZA. Notable concentrations of D_6 reach the ZA after 2 years, but trace quantities already arrive after about 270 days, having been mixed upward into the upper layer and transported southward in the Brazil Current. The offline simulations display qualitatively similar behavior, but D_5 inventories are significantly higher (+40%), with again significant sequestration below 1000 m. D_6 inventories are slightly lower (-7%) than in the online simulations, despite higher values above 1000 m.

Dye tracers D_3 and D_4, released at the eastern domain boundary, take much longer to reach the ZA due, to very low westward flow velocities in the interior part of the basin. Offline inventories of D_3 in the upper 1000 m are about 50% smaller than in the online simulation, a deficiency that can only be partly explained by sequestration below 1000 m. D_4 inventories are 65% too high, with enhanced stock both below and above 1000 m depth.

Based on the propagation speed of the diffusion front of D_1 in the offline simulation (Fig. 4a, center column), we can make a rough estimate of the artificial vertical diffusivity that is introduced by the advection issue. We are able to model the depth of the diffusion front below $z_0 = -1000$ m and after $t_0 = 132$ days as $z = z_0 - \sqrt{4D(t - t_0)}$, when $D = 1.74 \cdot 10^{-2} \text{m}^2/\text{s}$. This is 2 to 3 orders of magnitude larger than typical values for background diffusivity used in ocean models.
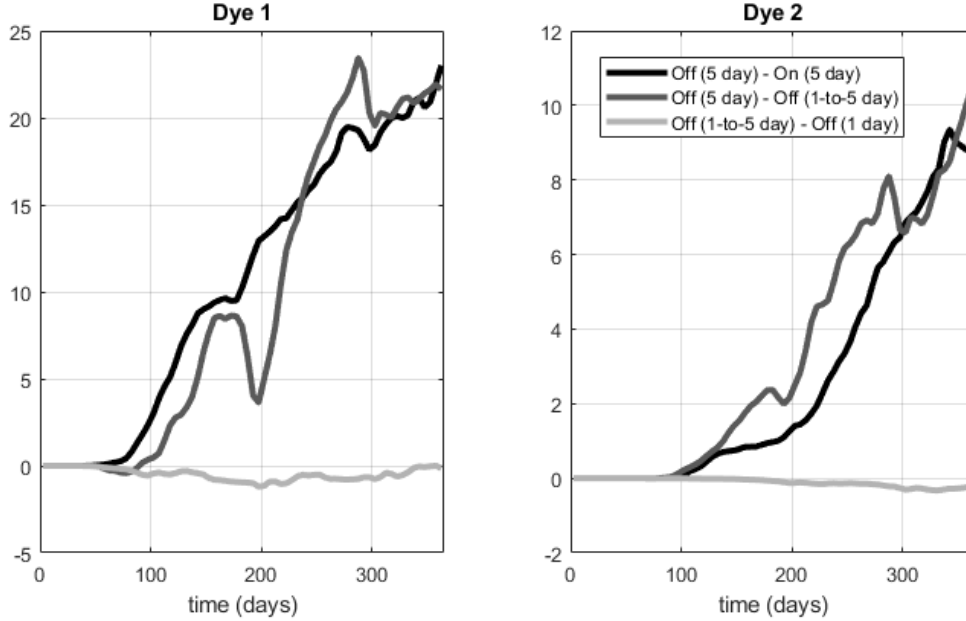
Figure 6. Comparison of inventories (10^{12} kg) of dye tracers D_1 and D_2 in the Zapiola Anticyclone for the original simulation with 5-day-averaged operators, and the alternate simulation with 1-day-averaged operators. Shown are the differences between the offline simulation using 5-day averaged operators and the corresponding online simulation (black); between the offline simulation using 5-day averaged operators, and the alternate offline simulation, with 1-day averaged operators averaged to 5 days (dark gray); and between the alternate offline simulations with 1-day averaged operators averaged to 5 days, and the 1-day averaged operators (light gray).

3.3 The Zapiola test case: The Role of Temporal Averaging

The impact of temporal averaging is investigated by comparing simulations with 1-day and 5-day averaged operators. To that end, we ran another online simulation for which we saved 1-day averaged IRFs. This simulation was run for 105 days, producing 105 operator sets. The offline simulations were run for 365 days, hence cycling through the operator set almost 3.5 times.

The online simulations that produced the 1-day and 5-day averaged operators were not bit-for-bit identical, as we inadvertently specified different processor counts. A positive consequence of this oversight is that we have two different realizations of the same chaotic system, allowing us to assess how the tracer advection error compares to trajectory divergence, in terms of their impact on tracer inventories. Figure 6 shows that averaging 1-day averaged operators to 5-day averages has a very small impact on the tracer inventories (light gray); the impact on spatial distributions is similarly small (not shown). This shows that 5-day averaged operators are sufficient to accurately reproduce tracer distributions. Comparison of the black and dark gray lines shows that the impact of trajectory divergence on tracer inventories (dark gray) is of similar magnitude as the impact of the advection error (black), at least for the first year of simulations.

14

Metric/Model	POP	FEOTS Regional	FEOTS Global (est.)
CPU-hours per sim. year	9020	47	2115
Sim. years per day	6.5	3	0.06
Cores Required	2432	6	6

Table 2. The computational costs, model throughput, and computational hardware requirements are compared for the online parent model (POP), a regional configuration of FEOTS, and the estimated expenses for a global offline FEOTS simulation.

3.4 Computational performance

290 The primary goal of FEOTS is to perform tracer calculations at significantly lower cost than the parent model. Additionally, FEOTS allows researchers to take advantage of transport operators produced by state-of-the-art climate simulations to conduct regional offline simulations. This provides flexibility in studying ocean transport phenomena and increases the value of online produced model data while considerably reducing the computational expense for researcher solely interested in studies involv-ing passive tracers. Here we evaluate the computational performance of a regional FEOTS configuration and compare it with
295 the global parent model.

The total cost of using FEOTS is associated with the following steps :

1. Impulse functions are generated from the model grid,

2. The impulse functions are then repeatedly passed through the passive tracer components of POP while running an online simulation,

300 3. The diagnosed IRFs are translated from gridded output to a sparse matrix format,

4. Offline passive tracer simulations are run

The first three steps are one-time costs that are necessary to generate the transport operator database. In our experience, Impulse function generation introduces a negligible cost, requiring only a few minutes to run in serial. Simulation of the passive tracers with the parent model to generate the impulse response functions requires about a factor of six more cpu-hours than when
305 running without tracers. This is the most significant up-front cost in generating the transport operator database. Diagnosis of the sparse matrices introduces a small cost; for the parent model presented here, about 15 minutes of wall-time on a single core is needed per transport operator. The expense of the offline passive tracer simulation depends on the specific use case. Below, we we provide an example below based on the Argentine Basin test problem and a simple global simulation.

Table 2 summarizes a comparison of the computational expense and compute platform size requirements between POP
310 and FEOTS. We ran the 0.3° ocean/sea ice configuration of E3SM-HiLAT on LANL's Institutional Computing clusters. A typical simulation with 6 dye tracers costs 9020 cpu-hrs per simulated year, using 2432 cores on 76 nodes. The throughput is 6.5 simulated years per wall-clock day. The simulation with 53 IRFs (in addition to the 6 dye tracers) typically costs 45,000 cpu-hrs, with a throughput of 1.60 simulated years per day when using 2912 cores.

15

Name	Percent Time
VerticalMixingAction	29.73%
VerticalMixingPrecondition	27.49%
VerticalMixing_POP_FEOTS	18.62%
CalculateTendency_TracerStorage	12.28%
DotProduct_POP_FEOTS	11.19%

Table 3. Flat profile of FEOTS showing the top five most expensive routines for an offline regional simulation

In contrast, a one-year offline FEOTS simulation of the Argentine Basin problem with 6 tracers takes roughly 47 cpu-hrs, and
315 a throughput of 3 simulated years per day on 6 cores. The iterative treatment of vertical mixing is most expensive, as a one-year
simulation without vertical mixing costs 6.8 cpu-hrs, and a throughput of 20 simulated years per day on 6 cores. To develop
an estimate for a global offline simulation with FEOTS, we assume that the cpu-hours scale linearly with the number of grid
cells. The Argentine Basin simulation has 1.02×10^6 grid cells, whereas a global configuration about 45 times more grid cells.
Thus, an offline simulation with FEOTS is expected to cost about 2115 cpu-hours per simulation year in the current version,
320 77% less cpu-hours than the parent model. However, the expected throughput for an offline global simulation is estimated as 1
model year for every 15 days.

In order for FEOTS to be a practical tool for simulating ocean tracers, the time-to-solution for transient simulations, and
ultimately steady-state simulations, needs to comparable to the ocean modelers current expectations. Our initial resource re-
quirement comparison with online simulations indicate that offline tracer simulations provide a viable approach towards eddy-
325 resolving ocean tracer modeling at a significantly reduced computational expense. However, the expected model throughput
for offline global simulations is two orders of magnitude lower than current online simulations, suggesting performance opti-
mizations needs to be explored in future development efforts of FEOTS.

Table 3 shows the five most expensive routines in FEOTS and the percentage of the total wall-time spent executing those
routines. Of those five, the top three are associated with the vertical mixing of dye tracers. The fourth most expensive routine
330 calculates the tendencies in the tracer fields due to ocean transport. All of these routines execute sparse matrix-vector multi-
plication in order to compute advective and diffusive tendencies. Currently, FEOTS implements all sparse matrix operations
in serial. Because of this, future efforts in reducing the time-to-solution of FEOTS simulation will likely focus on exposing
parallelism in sparse matrix-vector operations.

4   Discussion

335 Based on this work, we posit that offline tracer simulations provide a viable modeling capability at a significantly reduced
computational expense compared to online models. With the reduction in computational expense, however, we have shown
that the offline simulations can produce tracer distributions consistent with a more diffusive ocean circulation than online

16

models. A potential approach to mitigate this problem, when using nonlinear flux-limiting advection schemes, is to replace the impulse fields with smoother basis functions, as discussed by Khatiwala et al. (2005).

340 When using impulse fields with sharp discontinuities, the 3rd Order flux-limited Lax-Wendroff advection scheme reduces effectively to a first order upwind scheme. By leveraging smoother basis functions for the impulse fields with this scheme, a less diffusive advection operator can be diagnosed. Using a smoother basis function, however, is expected to introduce additional complications for diagnosing transport operators. In general, the process of diagnosing the transport operators can be thought of as a matrix projection problem,

345 $$\mathbb{A}\mathbb{F} = \mathbb{R} \tag{14}$$

where $\mathbb{A}$ is the transport operator we want to diagnose, $\mathbb{F}$ is a matrix whose columns are the impulse fields, and $\mathbb{R}$ is a matrix whose columns are the impulse response fields. The advection operator is obtained by multiplying (14) by the right-inverse of $\mathbb{F}$

$$\mathbb{A} = \mathbb{R}\mathbb{F}^{-1} \tag{15}$$

350 Ideally, the basis function we choose should be smooth enough to retain higher order terms in the 3rd Order flux-limited Lax-Wendroff advection scheme. For computational purposes, the basis functions would ideally be mutually orthonormal so that the inverse is easy to calculate,

$$\mathbb{F}^{-1} = \mathbb{F}^{T} \tag{16}$$

This approach, along with experimentation with other advection schemes, is planned for future work.

355 With regards to performance, FEOTS can provide offline tracer modeling capabilities at significantly reduced computational expense and with practical runtimes for regional simulations. Projected computational resource requirements (cpu-hours) were shown to be about 77% less than the online parent model. Runtimes for global simulations, however, indicate that parallelism FEOTS needs to be exposed before it is practical for this use case. Addressing the slow runtime for global offline simulations is critical for working towards a framework that allows for the calculation of steady state solutions within a practical amount

360 of time. Currently, our plan for reducing runtime is to implement sparse matrix operations in parallel using an MPI+OpenMP framework.

5   Conclusions

In this paper we introduced the Fast Equilibration of Ocean Tracers Software (FEOTS), which is an end-to-end set of tools to efficiently calculate tracer distributions on a global or regional sub-domain. In our example problem we diagnose transport

365 operators from an eddy-permitting configuration of the POP ocean model, and calculate the distribution of passive dye tracers in the Argentine Basin for a 5-year period. This demonstration shows the feasibility of this approach, while at the same time highlighting the limitations of the Impulse Response Functions approach in capturing tracer transports by a non-linear advection scheme.

References

Bardin, A., Primeau, F., and Lindsay, K.: An offline implicit solver for simulating prebomb radiocarbon, Ocean Modelling, 73, 45–58, 2014.

de Miranda, A. P., Barnier, B., and Dewar, W. K.: On the dynamics of the Zapiola Anticyclone, Journal of Geophysical Research: Oceans, 104, 21 137–21 149, 1999.

390 Dewar, W. K.: Topography and barotropic transport control by bottom friction, Journal of Marine Research, 56, 295–328, 1998.

Dukhovskoy, D. S., Myers, P. G., Platov, G., Timmermans, M.-L., Curry, B., Proshutinsky, A., Bamber, J. L., Chassignet, E., Hu, X., Lee, C. M., et al.: Greenland freshwater pathways in the sub-Arctic Seas from model experiments with passive tracers, Journal of Geophysical Research: Oceans, 121, 877–907, 2016.

Fu, L.-L. and Smith, R. D.: Global ocean circulation from satellite altimetry and high-resolution computer simulation, Bulletin of the Amer-
395 ican Meteorological Society, 77, 2625–2636, 1996.

Garzoli, S. L.: Geostrophic velocity and transport variability in the Brazil-Malvinas Confluence, Deep Sea Research Part I: Oceanographic Research Papers, 40, 1379–1403, 1993.

Griffies, S. M., Winton, M., Samuels, B., Danabasoglu, G., Yeager, S., Marsland, S., Drange, H., and Bentsen, M.: Datasets and protocol for the CLIVAR WGOMD Coordinated Ocean-sea ice Reference Experiments (COREs), WCRP Report, 21, 1–21, 2012.

400 Gu, S., Liu, Z., Jahn, A., Rempfer, J., Zhang, J., and Joos, F.: Modeling neodymium isotopes in the ocean component of the community earth system model (CESM1), Journal of Advances in Modeling Earth Systems, 11, 624–640, 2019.

Hallberg, R.: Using a resolution function to regulate parameterizations of oceanic mesoscale eddy effects, Ocean Modelling, 72, 92–103, 2013.

Hecht, M., Veneziani, M., Weijer, W., Kravitz, B., Burrows, S., Comeau, D., Hunke, E., Jeffery, N., Urrego-Blanco, J., Wang, H., et al.:
405 E3SMv0-HiLAT: A modified climate system model targeted for the study of high-latitude processes, Journal of Advances in Modeling Earth Systems, 11, 2814–2843, 2019.

Hecht, M. W., Hunke, E., Maltrud, M., Petersen, M. R., and Wingate, B. A.: Lateral mixing in the eddying regime and a new broad-ranging formulation, Eddy resolving ocean models, Geophysical Monograph, 177, 339–352, 2008.

Jahn, A., Lindsay, K., Giraud, X., Gruber, N., Otto-Bliesner, B. L., Liu, Z., and Brady, E. C.: Carbon isotopes in the ocean model of the
410 Community Earth System Model (CESM1), Geoscientific Model Development, 8, 2419–2434, 2015.

Jullion, L., Heywood, K. J., Naveira Garabato, A. C., and Stevens, D. P.: Circulation and water mass modification in the Brazil–Malvinas Confluence, Journal of Physical Oceanography, 40, 845–864, 2010.

Khatiwala, S.: A computational framework for simulation of biogeochemical tracers in the ocean, Global Biogeochemical Cycles, 21, 2007.

Khatiwala, S., Visbeck, M., and Cane, M. A.: Accelerated simulation of passive tracers in ocean circulation models, Ocean Modelling, 9,
415 51–69, 2005.

Khatiwala, S., Primeau, F., and Hall, T.: Reconstruction of the history of anthropogenic CO_2 concentrations in the ocean, Nature, 462, 346–349, 2009.

Lozier, M. S.: Deconstructing the conveyor belt, science, 328, 1507–1511, 2010.

Missiaen, L., Menviel, L. C., Meissner, K. J., Roche, D. M., Dutay, J.-C., Bouttes, N., Lhardy, F., Quiquet, A., Pichat, S., and Waelbroeck,
420 C.: Modelling the impact of biogenic particle flux intensity and composition on sedimentary Pa/Th, Quaternary Science Reviews, 240, 106 394, 2020.

Mountford, A. and Morales Maqueda, M.: Eulerian modeling of the three-dimensional distribution of seven popular microplastic types in the global ocean, Journal of Geophysical Research: Oceans, 124, 8558–8573, 2019.

Primeau, F.: Characterizing transport between the surface mixed layer and the ocean interior with a forward and adjoint global ocean transport
425   model, Journal of Physical Oceanography, 35, 545–564, 2005.

Ringler, T., Petersen, M., Higdon, R. L., Jacobsen, D., Jones, P. W., and Maltrud, M.: A multi-resolution approach to global ocean modeling, Ocean Modelling, 69, 211–232, 2013.

Sarmiento, J. L., Orr, J. C., and Siegenthaler, U.: A perturbation simulation of CO2 uptake in an ocean general circulation model, Journal of Geophysical Research: Oceans, 97, 3621–3645, 1992.

430   Saunders, P. M. and King, B. A.: Bottom currents derived from a shipborne ADCP on WOCE cruise A11 in the South Atlantic, Journal of Physical Oceanography, 25, 329–347, 1995.

Séférian, R., Berthet, S., Yool, A., Palmieri, J., Bopp, L., Tagliabue, A., Kwiatkowski, L., Aumont, O., Christian, J., Dunne, J., et al.: Tracking improvement in simulated marine biogeochemistry between CMIP5 and CMIP6, Current Climate Change Reports, pp. 1–25, 2020.

Shewchuk, J. R.: An Introduction to the Conjugate Gradient Method Without the Agonizing Pain, Tech. rep., School of Computer Science,
435   Carnegie Mellon University, http://www.cs.cmu.edu/~quake-papers/painless-conjugate-gradient.pdf, 1994.

Smith, R., Jones, P., Briegleb, B., Bryan, F., Danabasoglu, G., Dennis, J., Dukowicz, J., Eden, C., Fox-Kemper, B., Gent, P., Hecht, M., Jayne, S., Jochum, M., Large, W., Lindsay, K., Maltrud, M., Norton, N., Peacock, S., Vertenstein, M., and Yeager, S.: The Parallel Ocean Program (POP) reference manual: Ocean component of the Community Climate System Model (CCSM), Tech. rep., Los Alamos National Laboratory, http://nldr.library.ucar.edu/repository/collections/OSGC-000-000-000-954, 2010.

440   Wang, S., Moore, J., Primeau, F., and Khatiwala, S.: Simulation of anthropogenic CO2 uptake in the CCSM3. 1 ocean circulation-biogeochemical model: comparison with data-based estimates, Biogeosciences, 9, 1321–1336, 2012.

Weijer, W., Maltrud, M. E., Homoky, W. B., Polzin, K. L., and Maas, L. R.: Eddy-driven sediment transport in the Argentine Basin: Is the height of the Zapiola Rise hydrodynamically controlled?, Journal of Geophysical Research: Oceans, 120, 2096–2111, 2015.

Weijer, W., Barthel, A., Veneziani, M., and Steiner, H.: The Zapiola Anticyclone: A Lagrangian study of its kinematics in an eddy-permitting
445   ocean model, Deep Sea Research Part I: Oceanographic Research Papers, 164, 103 308, 2020.

Zhang, J., Liu, Z., Brady, E. C., Oppo, D. W., Clark, P. U., Jahn, A., Marcott, S. A., and Lindsay, K.: Asynchronous warming and $\delta 18O$ evolution of deep Atlantic water masses during the last deglaciation, Proceedings of the National Academy of Sciences, 114, 11 075–11 080, 2017.

Zhang, J., Weijer, W., Maltrud, M. E., Veneziani, C., Jeffery, N., Hunke, E. C., Urrego Blanco, J. R., and Wolfe, J. D.: An eddy-permitting
450   ocean-sea ice general circulation model (E3SMv0-HiLAT03): Description and evaluation, Tech. rep., Los Alamos National Lab.(LANL), Los Alamos, NM (United States), https://doi.org/10.2172/1542803, 2019.

Zhang, J., Weijer, W., Steele, M. A., Cheng, W., Verma, T., and Veneziani, M.: Labrador Shelf freshening linked to Beaufort Gyre freshwater release, Nature Communications, in press, 2021.